A Space-Time Finite Element Method for the Exterior Acoustics Problem

Lonny L. Thompson

Department of Mechanical Engineering, Clemson University
Clemson, South Carolina 29634-0921

Peter M. Pinsky

Department of Civil Engineering, Stanford University
Stanford, California 94305-4020

Abstract

In this paper, the development of a space-time finite element method for solution of the transient acoustics problem in exterior domains is discussed. The space-time formulation for the exterior acoustics problem is obtained from a time-discontinuous Galerkin variational equation for coupled structural acoustics, specialized to the case of zero normal velocities on the wet surface, i.e., a rigid scatterer. The formulation employs a finite computational acoustic domain surrounding the scatterer and incorporates high-order time-dependent non-reflecting (radiation) boundary conditions on the fluid truncation boundary as 'natural' boundary conditions in the space-time variational equation, i.e. they are enforced weakly in both space and time. The result is an algorithm for direct transient analysis of acoustic radiation and scattering with the desired combination of good stability and high accuracy. The method is especially useful for the application of adaptive solution strategies for transient acoustics in which unstructured space-time meshes are used to track wave fronts propagating along space-time characteristics. Optimal stability estimates and convergence rates are reported together with two representative numerical examples involving transient radiation and scattering which illustrate the high-order accuracy achieved by the method for the exterior acoustics problem.

PACS numbers: 43.20.Px, 43.20.Tb

The Journal of the Acoustical Society of America,
June 1, 1996, Volume 99, Issue 6, pp.3297-3311

(Received 14 August 1994; accepted 25 October 1995; revised 3 October 1995)

1 Introduction

For linear problems characterized by a relatively small range of frequencies, a transient solution may be obtained indirectly through a sequence of time-harmonic solutions in the frequency domain followed by an inverse Fourier transform. Considerable progress has been made in the development of numerical methods for the time-harmonic exterior structural acoustics problem. Still, a direct time-domain approach is necessary whenever nonlinearities occur and may be advantageous for some classes of linear problems including real-time dynamic control and optimization. For example, in problems characterized by broad frequency spectrums, such as short pulse wave propagation, the indirect approach may not be computationally feasible since it requires a large number of solutions in the frequency domain for any reasonably accurate sweep of the problem band width. Previous direct time-domain approaches to the transient structural acoustics problem involving the interaction of vibrating structures submerged in an infinite acoustic fluid have employed (i) boundary element methods based on Kirchhoff's retarded potential integral formulation, e.g. [1, 2, 3, 4, 5], (ii) Taylor-Galerkin methods, e.g. [6], and (iii) semi-discrete methods which employ standard Galerkin finite element methods in space and classical finite difference techniques for integrating in time (also referred to as the method of lines), see e.g. [7, 8, 9, 10, 11]. However for general transient wave propagation problems it is known that these standard methods are not optimal. This is especially evident for problems involving sharp gradients in the solution which typically arise in the vicinity of fluid-structure interfaces near inhomogeneities such as stiffeners and structural joints, and abrupt changes in geometry.

In this paper a space-time finite element formulation for solving the transient acoustics problem in exterior domains is described. The formulation is based on the time-discontinuous Galerkin finite element method for general second-order hyperbolic equations described in [12, 13], in the context of elastodynamics. The starting point for application of this methodology to the exterior acoustics problem is the time-discontinuous Galerkin variational equation for the coupled fluid-structure system derived in [14, 15], specialized here to the case of a rigid scatterer, i.e., the normal velocity is set to zero on the wet surface. In this approach, the concept of space-time slabs is employed which allow for discretizations that are discontinuous in time and offers great flexibility in the discretization; in particular through the possibility of using space-time meshes oriented along space-time characteristics. The resulting space-time algorithm gives a general solution to the fundamental problem of constructing a finite element method for transient acoustics with the desired combination of good stability and high accuracy. Stability is obtained through the introduction of temporal jump operators which give rise to a natural high-frequency dissipation required for the accurate resolution of sharp gradients in the physical solution. Additional stability may be obtained by a least-squares modification, i.e. Galerkin Least Squares (GLS) stabilization. The order of accuracy of the solution is related to the order of

the finite element spatial and temporal basis functions chosen, and can be specified to any accuracy and for general unstructured discretizations in space and time.

In addition to the advantages cited above, the space-time finite element approach provides a powerful framework for unified and simultaneous spatial and temporal adaptivity of the discretization. This is especially useful in the application of self-adaptive solution strategies for transient structural acoustics, in which both spatial and temporal enhancement can efficiently capture waves propagating along space-time characteristics. Furthermore the use of space-time hp-adaptive discretization strategies, where a combination of mesh size refinement/unrefinement (h-adaptivity), and finite element basis enrichment (p-adaptivity), can easily be accommodated in the time-discontinuous formulation. Because the temporal and spatial domains are treated in a consistent manner in the space-time variational equations, the method gives rise to a firm mathematical foundation from which rigorous *a posteriori* error estimates useful for reliable and efficient adaptive schemes may be established, see e.g. [16].

The time-discontinuous Galerkin method is also referred to as the Discontinuous Galerkin (DG) method in time and was first introduced by Lesaint and Raviart [17] in the context of first-order neutron transport equations. DG space-time methods with residual based stabilization such as Galerkin Least Squares (GLS), Streamline Diffusion (SD) and Streamline Upwind Petrov-Galerkin (SUPG) methods in the context of fluid flows, have successfully been applied to first-order hyperbolic/parabolic systems of partial differential equations by Johnson, Hughes and colleages, and others, see e.g. [18, 19, 20]. Stabilized methods of this type are now widely used in many applications arising in computational fluid dynamics (CFD), including problems governed by the compressible Euler and Navier-Stokes equations [21, 22, 23], advection-diffusion problems [24], and large-eddy and turbulence modeling [25].

Classical linear acoustics equations can be converted to first-order hyperbolic form and these methods are thus immediately applicable. However, in this approach, the coupled state vector consists of acoustic pressure and velocity components, which is computationally uneconomical. Hughes and Hulbert [12, 13] have successfully extended the time-discontinuous Galerkin space-time method originally designed for first-order systems to second-order hyperbolic equations in the context of transient elastodynamics. Based on the success of the work in [12], this technology has recently been used by the authors to develop a time-discontinuous Galerkin variational formulation for the structural acoustics problem involving the second-order wave equation governing acoustics coupled to the the elastodynamics equations governing the structure; see [14, 15, 26]. For the coupled equations, scalar velocity potential is used as the solution variable for the acoustic fluid, while the displacement vector is used to represent the structure. As a consequence of this choice of variables, the coupled time-discontinuous Galerkin variational equations for structural acoustics give rise to a positive matrix form, which in the context of the space-time finite element formulation, allows for the proof of the algorithmic stability and convergence

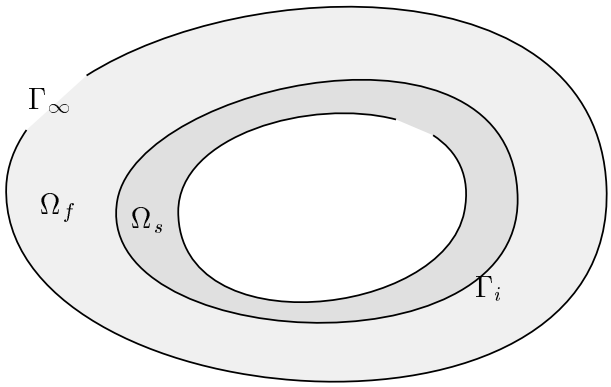

Fig. 1: Coupled system for the exterior problem, with artificial boundary Γ_∞ enclosing the finite domain $\Omega = \Omega_f \cup \Omega_s$.

of the method. In this paper, attention is focused on the stability and accuracy of the time-discontinuous Galerkin method for the exterior acoustic fluid coupled with the second-order non-reflecting boundary condition originally derived by Bayliss and Turkel in [27]; or equivalently, the time-dependent counterpart to the local second-order operator in the truncated Dirichlet-to-Neumann (DtN) map given [14, 28]. In Section 2 the governing equations for the exterior acoustics problem are summarized. In Sections 3 and 4, the space-time variational equation is presented together with a discussion of the form of the resulting matrix equations. In Sections 5, 6, and 7, results are reported from a stability and convergence analysis of the method. In Section 8, we undertake a brief development of the high-order accurate time-dependent radiation boundary conditions developed in [14, 28], together with a discussion of their relationship to the local radiation boundary conditions of Bayliss and Turkel, and characterize their accuracy when implemented in the space-time finite element formulation for transient acoustics.

2 The Exterior Acoustics Problem

The exterior acoustics problem in an infinite domain is transformed to a problem defined over a finite computational domain through the introduction of an artificial fluid truncation boundary. Radiation boundary conditions are prescribed on the fluid truncation boundary in the form of linear operators which approximate the asymptotic behavior of the outgoing solution at infinity.

The computational fluid domain is denoted by Ω_f with boundary $\partial\Omega_f$, divided into the artificial truncation boundary Γ_∞, and the surface of the scatterer, denoted Γ_i. The infinite domain outside the artificial boundary is denoted by Ω_∞. For an elastic scatterer, the interface Γ_i, seperates the fluid domain from a structural domain Ω_s; see Figure 1. The unit inward normal to Ω_f on Γ_i, and the unit outward normal

to Ω_f on Γ_∞ is denoted by $\boldsymbol{n}$. The temporal interval of interest is $I =]0, T[$ and the number of spatial dimensions is n_{sd}.

The fluid is assumed under the usual conditions for linear acoustics, namely an inviscid, and compressible fluid with small disturbance from a reference state. From the assumption of an irrotational acoustic fluid, the velocity of the fluid can be written as the gradient of the velocity potential $\phi(\boldsymbol{x}, t)$ with $\boldsymbol{x} \in \Omega_f$ as $\boldsymbol{v}_f = \nabla\phi$. Consequently, acoustic pressure is related to the velocity potential by $p = -\rho_f \dot{\phi}$, and the motion of the fluid can be modeled by the scalar wave equation:

$$\nabla^2\phi - a^2\ddot{\phi} \quad = \quad f \qquad \text{in} \;\; Q_f \equiv \Omega_f \times I \tag{1}$$

The phase velocity is denoted by $c > 0$, with slowness $a = c^{-1}$ and $\rho_f > 0$ is the reference density for the fluid. The acoustic source loading is given by f. A superposed dot indicates partial differentiation with respect to time t.

On the interface Γ_i, the normal component of the fluid velocity is assumed to be equivalent to the motion of the surface. Projecting the velocity normal to the surface gives: $\nabla\phi \cdot \boldsymbol{n} = \boldsymbol{v} \cdot \boldsymbol{n}$ on Γ_i where $\boldsymbol{v}$ is a given function in time on Γ_i. For an elastic body coupled to the fluid, $\boldsymbol{v}(\boldsymbol{x}\,, t)$ with $\boldsymbol{x} \in \Omega_s$ is the structural velocity vector. The influence of the fluid pressure acting on an elastic structure is given by the normal traction $\boldsymbol{\sigma} \cdot \boldsymbol{n} = -p\boldsymbol{n}$ where $\boldsymbol{\sigma} = \boldsymbol{\sigma}(\nabla \boldsymbol{u})$ is the symmetric Cauchy stress tensor which is a function of the structural displacements $\boldsymbol{u}$, such that $\boldsymbol{v} = \dot{\boldsymbol{u}}$. For a rigid scatterer, the structural displacement is zero and $\boldsymbol{v} = 0$, $\forall\, t \in I$, so that the boundary condition on Γ_i specializes to $\nabla\phi \cdot \boldsymbol{n} = 0$.

Initial conditions for the second-order hyperbolic equation governing the acoustic fluid are:

$$\phi(\boldsymbol{x}, 0) \quad = \quad \phi_0(\boldsymbol{x}) \qquad \dot{\phi}(\boldsymbol{x}, 0) \quad = \quad \dot{\phi}_0(\boldsymbol{x}) \qquad\qquad \boldsymbol{x} \in \Omega_f \tag{2}$$

For an elastic solid, initial conditions on the structural displacement and velocity are also prescribed.

On the artificial boundary Γ_∞ boundary conditions are specified which approximate the asymptotic behavior of the solution at infinity as described by the Sommerfeld radiation condition. For Γ_∞ taken to be a sphere in three spatial dimensions $\mathbb{R}^{n_{sd}} = \mathbb{R}^3$, the obvious choice is to use a simple Sommerfeld-like boundary condition of the form,

$$\nabla\phi \cdot \boldsymbol{n} \quad = \quad -a\dot{\phi} \qquad\qquad \text{on} \quad \Upsilon_\infty := \Gamma_\infty \times]0, T[\tag{3}$$

where $\nabla\phi \cdot \boldsymbol{n} = \partial\phi/\partial n$ is the normal derivative on Γ_∞. Restated in terms of pressure, $p = -\rho_f\dot{\phi}$, and velocity $\boldsymbol{v}_f = \nabla\phi$, equation (3) becomes,

$$\boldsymbol{v}_f \cdot \boldsymbol{n} = p/z_o \tag{4}$$

where $z_o = \rho_f c$, is the characteristic impedance for plane-wave propagation. This boundary condition is exact in one-dimension for any position, however in multi-dimensions, when (3) is applied at a finite distance from the source of excitation,

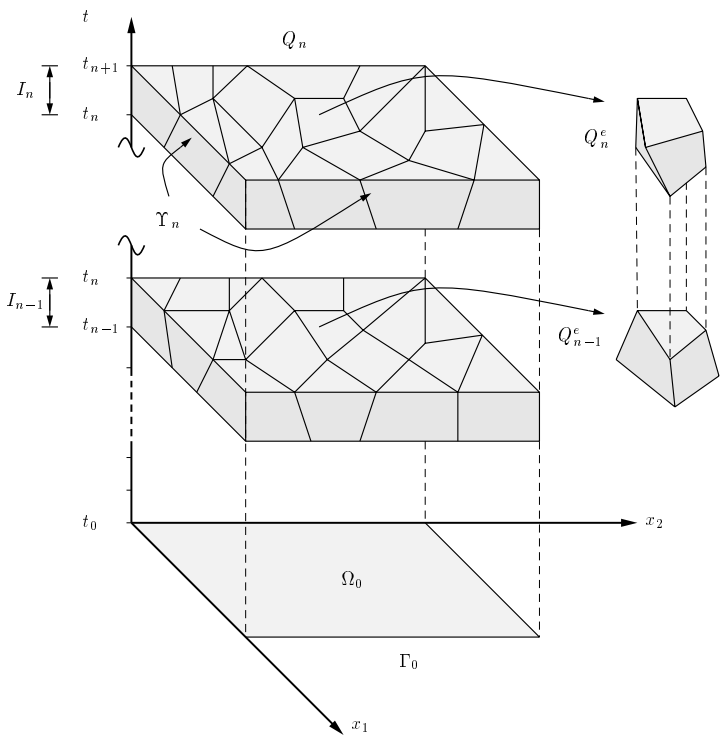

Fig. 2: Illustration of two consecutive space-time slabs with unstructured finite element meshes in space-time.

this boundary condition will generally produce large spurious reflections, resulting in unacceptable errors in the numerical solution, see e.g. [10]. Because of the potential loss of accuracy resulting from the use of (3), an improved non-reflecting boundary is needed. A number of high-order accurate non-reflecting boundary conditions are available and can take several different forms depending on the local (differential) or nonlocal (integral) operators appearing in their definition.

An example of a local operator is the first-order boundary condition,

$$\frac{\partial \phi}{\partial n} = -\mathbb{S}_1 \phi, \qquad \text{where} \quad \mathbb{S}_1 := \frac{1}{R} + a\frac{\partial}{\partial t} \tag{5}$$

where R is the radial distance to a spherical boundary Γ_∞. This well-known radiation boundary condition is referred to as a 'spherical damper' since this operator completely absorbs radially symmetric spherical waves. In Section 8, higher-order radiation boundary conditions are reviewed which absorb radially symmetric and higher-order spherical wave harmonics on Γ_∞.

3 Space-time finite element formulation

The development of the space-time method for transient acoustics proceeds by considering a partition of the time interval, $I =]0, T[$, of the form: $0 = t_0 < t_1 < \cdots < t_N = T$, with $I_n =]t_n, t_{n+1}[$. Using this notation, $Q_n^f = \Omega_f \times I_n$ denotes the nth space-time slab for the fluid. When an elastic solid is coupled to the fluid, the nth space-time slab for the structural region is denoted by $Q_n^s = \Omega_s \times I_n$. For the nth space-time slab, the spatial domain is subdivided into $(n_{el})_n$ elements, and the interior of the e^{th} element is defined as Q_n^e. Figure 2 shows an illustration of two consecutive space-time slabs Q_{n-1} and Q_n for the fluid where the superscript is omitted for clarity.

Within each space-time element, the trial solution and weighting function are approximated by pth-order polynomials in $\boldsymbol{x}$ and t. These functions are assumed $C^0(Q_n)$ continuous throughout each space-time slab, but are allowed to be discontinuous across the interfaces of the slabs. This feature is implemented through the use of discontinuous temporal jump terms at each space-time slab interface,

$$[\![\phi^h(t_n)]\!] \quad = \quad \phi^h(\boldsymbol{x}\,,\, t_n^+) \,-\, \phi^h(\boldsymbol{x}\,,\, t_n^-)$$

These jump operators weakly enforce initial conditions across time slabs and allows for the general use of high-order elements and spectral-type interpolations in both space and time. The specific form of these jump operators are designed such that a natural norm emanates from the variational equation and satisfies a strong coercivity condition. From a Fourier analysis, it can be shown that the jump operators introduce beneficial numerical dissipation for frequencies above the spatial resolution limit.

For the acoustic fluid, the collection of finite element basis functions are given by the space of trial velocity potentials,

Trial fluid potential

$$\mathcal{T}^h = \bigcup_{n=0}^{N-1} \mathcal{T}_n^h\,, \qquad \mathcal{T}_n^h \quad = \quad \left\{ \phi^h(\boldsymbol{x},t) \middle| \phi^h \in C^0(Q_n^f)\,,\, \phi^h\Big|_{Q_n^{f^e}} \in \mathcal{P}^p(Q_n^{f^e}) \right\}$$

where $\mathcal{P}^p$ denotes the space of pth-order polynomials and C^0 denotes the space of continuous functions. For an elastic solid coupled to the fluid, the space of trial functions $\mathcal{S}^h = \bigcup_{n=0}^{N-1} \mathcal{S}_n^h$, for the structural displacements is defined in [12, 14, 15], and has similar restrictions on continuity.

Before stating the space-time variational equations, it is useful to introduce the

following notation.

$$
\begin{aligned}
(\boldsymbol{w}^h\,,\,\boldsymbol{u}^h)_{\Omega_s} &= \int_{\Omega_s} \boldsymbol{w}^h \cdot \boldsymbol{u}^h \, d\Omega \\
a(\boldsymbol{w}^h\,,\,\boldsymbol{u}^h)_{\Omega_s} &= \int_{\Omega_s} \nabla \boldsymbol{w}^h \cdot \boldsymbol{\sigma}(\nabla \boldsymbol{u}^h) \, d\Omega \\
(w^h\,,\,\phi^h)_{\Omega_f} &= \int_{\Omega_f} w^h \, \phi^h \, d\Omega \\
(w^h\,,\,\phi^h)_{\Gamma} &= \int_{\Gamma} w^h \, \phi^h \, d\Gamma \\
(w^h\,,\,\phi^h)_{Q_n} &= \int_{t_n}^{t_{n+1}} (w^h\,,\,\phi^h)_{\Omega} \, dt
\end{aligned}
$$

The meaning of other similar terms may be inferred from these. The L_2 norm is denoted by $||\phi||_{\Omega} = (\phi\,,\,\phi)_{\Omega}^{1/2}$

4 Discontinuous Galerkin Space-Time Variational Equation

The space-time variational formulation is obtained from a weighted residual of the governing equations and incorporates time-discontinuous jump terms. The specific form of this time-discontinuous Galerkin formulation is designed such that unconditional stability for arbitrary space-time finite element discretizations can be proved through a functional analysis of the method. The variational equation for the coupled structural acoustics problem derived in [14, 15] is presented first. The exterior acoustics problem is then obtained as a special case by setting the structural displacements and velocities to zero. The coupled space-time variational equation can be stated as: Within each space-time slab, $n = 0, 1, ..., N-1$; Find the trial solution $(\boldsymbol{u}^h\,,\,\phi^h) \in \mathcal{S}_n^h \times \mathcal{T}_n^h$, such that $\forall$ weighting functions $(\boldsymbol{w}^h\,,\,w^h) \in \mathcal{S}_n^h \times \mathcal{T}_n^h$:

$$
G_f(w^h\,,\,\boldsymbol{u}^h\,,\,\phi^h)_n + G_s(\boldsymbol{w}^h\,,\,\boldsymbol{u}^h\,,\,\phi^h)_n + G_{\infty}(w^h\,,\,\phi^h)_n = 0 \tag{6}
$$

where

$$
G_f(w^h\,,\,\boldsymbol{u}^h\,,\,\phi^h)_n = B_f(w^h\,,\,\phi^h)_n + \int_{t_n}^{t_{n+1}} \left(\dot{w}^h\,,\,\rho_f \dot{\boldsymbol{u}}^h \cdot \boldsymbol{n}\right)_{\Gamma_i} dt \tag{7}
$$

$$
G_s(\boldsymbol{w}^h\,,\,\boldsymbol{u}^h\,,\,\phi^h)_n = B_s(\boldsymbol{w}^h\,,\,\boldsymbol{u}^h)_n - \int_{t_n}^{t_{n+1}} \left(\dot{\boldsymbol{w}}^h \cdot \boldsymbol{n}\,,\,\rho_f \dot{\phi}^h\right)_{\Gamma_i} dt \tag{8}
$$

and

$$
\begin{aligned}
B_f(w^h\,,\,\phi^h)_n \quad &= \quad \int_{t_n}^{t_{n+1}} \left(\dot{w}^h\,,\,\rho_f a^2 \ddot{\phi}^h\right)_{\Omega_f} dt \,+\, \int_{t_n}^{t_{n+1}} \left(\nabla \dot{w}^h\,,\,\rho_f \nabla \phi^h\right)_{\Omega_f} dt \\
&+ \quad \left(\dot{w}^h(t_n^+)\,,\,a^2\,\rho_f [\![\dot{\phi}^h(t_n)]\!]\right)_{\Omega_f} \,+\, \left(\nabla w^h(t_n^+)\,,\,\rho_f [\![\nabla \phi^h(t_n)]\!]\right)_{\Omega_f} \\
&- \quad \int_{t_n}^{t_{n+1}} \left(\dot{w}^h\,,\,\rho_f f\right)_{\Omega_f} dt \qquad (9) \\
B_s(\boldsymbol{w}^h\,,\,\boldsymbol{u}^h)_n \quad &= \quad \int_{t_n}^{t_{n+1}} \left(\dot{\boldsymbol{w}}^h\,,\,\rho_s \ddot{\boldsymbol{u}}^h\right)_{\Omega_s} dt \,+\, \int_{t_n}^{t_{n+1}} a(\dot{\boldsymbol{w}}^h\,,\,\boldsymbol{u}^h)_{\Omega_s}\, dt \\
&+ \quad (\dot{\boldsymbol{w}}^h(t_n^+)\,,\,\rho_s [\![\dot{\boldsymbol{u}}^h(t_n)]\!])_{\Omega_s} \,+\, a(\boldsymbol{w}^h(t_n^+)\,,\,[\![\boldsymbol{u}^h(t_n)]\!])_{\Omega_s} \qquad (10)
\end{aligned}
$$

In the operator G_f, the terms evaluated over $\Omega_f \times I_n$, weakly enforce the scalar wave equation over the interior domain of the space-time slab. Fluid-structure interaction is accomplished through the coupling operators defined on the interface $\Gamma_i \times I_n$. For an elastic solid the momentum balance in the structure is enforced through the operator B_s, evaluated over $\Omega_s \times I_n$. The reference density for the structure is denoted ρ_s.

For a rigid structure, the normal velocity is zero, and the coupled variational equation (6) reduces to

$$
B_f(w^h\,,\,\phi^h)_n \,+\, G_\infty(w^h\,,\,\phi^h)_n \quad = \quad 0 \qquad (11)
$$

For the exterior problem, the operator G_∞, incorporates the time-dependent radiation boundary conditions on Γ_∞. The radiation boundary conditions are incorporated as natural boundary conditions in the variational equation, i.e., they are enforced weakly through integration over both the artificial boundary Γ_∞ and the time interval I_n. For the spherical damper $\mathbb{S}_1$, defined earlier in (5), the boundary operator is given by,

$$
\begin{aligned}
G_\infty(w^h\,,\,\phi^h)_n \quad &= \quad \frac{\rho_f}{R} \int_{t_n}^{t_{n+1}} (\dot{w}^h\,,\,\phi^h)_{\Gamma_\infty}\, dt \,+\, \frac{\rho_f}{c} \int_{t_n}^{t_{n+1}} (\dot{w}^h\,,\,\dot{\phi}^h)_{\Gamma_\infty}\, dt \\
&+ \quad \frac{\rho_f}{R} (w^h(t_n^+)\,,\,[\![\phi^h(t_n)]\!])_{\Gamma_\infty} \qquad (12)
\end{aligned}
$$

The implementation of higher-order boundary conditions will be described in Section 8.

The method is applied in one space-time slab at a time; data from the end of the previous slab are employed as initial conditions for the current slab. Matrix equations are obtained by introducing space-time finite element approximations for the primary variables. For the coupled structural acoustics problem the velocity potential and structural displacements are approximated as $\phi^h(\boldsymbol{x}\,,\,t) = \boldsymbol{N}_f(\boldsymbol{x}\,,\,t)\boldsymbol{\phi}$,

and $\boldsymbol{u}^h(\boldsymbol{x}\,,\,t) = \boldsymbol{N}_s(\boldsymbol{x}\,,\,t)\boldsymbol{d}$, respectively. In these expressions $\boldsymbol{N}_f \in \mathcal{T}_n^h$ and $\boldsymbol{N}_s \in \mathcal{S}_n^h$ are basis functions restricted to Q_n^f and Q_n^s respectively, and $\boldsymbol{d}$ and $\boldsymbol{\phi}$ are global solution vectors defined over a space-time slab. Inserting these expressions into the variational equation (6) leads to the coupled system of algebraic equations to be solved in sequence for each time interval $I_n =]t_n\,,\,t_{n+1}[,\ n = 0, 1, \cdots N-1$:

$$\begin{bmatrix} \boldsymbol{K}_s & \boldsymbol{A} \\ \boldsymbol{A}^T & \boldsymbol{K}_f \end{bmatrix} \begin{Bmatrix} \boldsymbol{d} \\ \boldsymbol{\phi} \end{Bmatrix} = \begin{Bmatrix} \boldsymbol{0} \\ \boldsymbol{f} \end{Bmatrix} \tag{13}$$

where $\boldsymbol{K}_f$ is the matrix emanating from the fluid operator B_f together with the radiation boundary operator G_∞, and $\boldsymbol{K}_s$ is the matrix emanating from the structural operator B_s. The off-diagonal partition $\boldsymbol{A}$ is the fluid-structure coupling matrix;

$$\boldsymbol{A} \quad = \quad \int_{t_n}^{t_{n+1}} \int_{\Gamma_i} \rho_f \boldsymbol{N}_{s,t}^T \boldsymbol{n} \boldsymbol{N}_{f,t}\ d\Gamma\ dt \tag{14}$$

In [26] it is shown that the coupled matrix system (13) is positive-definite; defining a unique solution for $\boldsymbol{d}$ and $\boldsymbol{\phi}$ for $n = 0, 1, 2, \cdots$. For the uncoupled exterior acoustics problem, the structure is assumed rigid, so that $\boldsymbol{d} = \boldsymbol{0}$, and (13) reduced to the positive matrix system;

$$\boldsymbol{K}_f\,\boldsymbol{\phi} = \boldsymbol{f} \tag{15}$$

The algorithm resulting from this space-time finite element approach can be contrasted with standard semidiscrete finite element methods where basis functions are defined in the spatial coordinate only, leaving a system of ordinary differential equations to be integrated in time; see e.g. [7, 8, 9, 10, 11] for applications of the semidiscrete finite element method to the exterior structural acoustics problem.

5 Stability Results

Results are summarized from a stability analysis of the space-time finite element formulation for the exterior structural acoustics problem performed in [14, 15]. These results are then specialized for the case of a rigid scatterer. In the absence of forcing terms, i.e., $f = 0$, and for $\mathbb{S}_1$, it has been proved in [14, 15] that the following energy decay inequality holds for the coupled space-time formulation:

$$\begin{aligned} &\mathcal{E}_s(\boldsymbol{u}^h(t_{n+1}^-)) \ + \ \mathcal{E}_f(\phi^h(t_{n+1}^-)) + \frac{1}{2R}||\phi^h(t_{n+1}^-)||_{\Gamma_\infty}^2 + \frac{1}{c}\int_0^{t_{n+1}} ||\dot{\phi}^h(t)||_{\Gamma_\infty}^2\ dt \\ \leq\ &\mathcal{E}_s(\boldsymbol{u}_0)) \ + \ \mathcal{E}_f(\phi_0)) \end{aligned} \tag{16}$$

for $n = 0, 1, 2, \cdots, N-1$. In the above $\mathcal{E}_s$ and $\mathcal{E}_f$ denote the energy for the elastic structure and acoustic fluid respectively, i.e.

$$\mathcal{E}_s(\boldsymbol{u}) \quad = \quad \frac{1}{2}\,(\dot{\boldsymbol{u}}\,,\,\rho_s\dot{\boldsymbol{u}})_{\Omega_s} \ + \ \frac{1}{2}\,a(\boldsymbol{u}\,,\,\boldsymbol{u})_{\Omega_s} \tag{17}$$

$$\mathcal{E}_f(\phi^h) \quad = \quad \frac{1}{2}\,\rho_f\,||a\dot{\phi}^h||^2_{\Omega_f} \;+\; \frac{1}{2}\,\rho_f\,||\nabla\phi^h||^2_{\Omega_f} \tag{18}$$

Equation (16) states that the total energy in the fluid-structure system, plus the energy absorbed through the radiation boundary, is always less than, or equal to the initial energy in the system. For a rigid scatterer, the structural displacements and velocities are zero, and (16) reduces to:

$$\mathcal{E}_f(\phi^h(t^-_{n+1})) + \frac{1}{2R}||\phi^h(t^-_{n+1})||^2_{\Gamma_\infty} + \frac{1}{c}\int_0^{t_{n+1}} ||\dot{\phi}^h(t)||^2_{\Gamma_\infty}\; dt \leq \mathcal{E}_f(\phi_0)) \tag{19}$$

Results (16) and (19) imply that *the space-time formulation presented is unconditionally stable.*

6 Galerkin Least Squares Stabilization

For additional stability, local residuals of the governing differential equations in the form of least-squares may be added to the Galerkin variational equations. The Galerkin Least Squares (GLS) addition to the variational equation for the acoustic fluid (7) is,

$$\begin{aligned} G^f_{GLS}(w^h\,,\,\phi^h)_n \;&=\; G_f(w^h\,,\,\phi^h)_n \;+\; (\rho_f c^2 \tau \mathcal{L}_1 w^h\,,\,(\mathcal{L}_1\phi^h - f))_{\tilde{Q}^f_n} \\ &+\; (\rho_f c^2 s \mathcal{L}_2 w^h\,,\,\mathcal{L}_2\phi^h)_{(\tilde{\Upsilon}_\infty)_n} \;+\; (\rho_f c^2 s \mathcal{L}_3 w^h\,,\,\mathcal{L}_3\phi^h)_{(\tilde{\Upsilon}_i)_n} \\ &+\; (\rho_f c^2 s [\![w^h_{,n}(\boldsymbol{x})]\!]\,,\,[\![\phi^h_{,n}(\boldsymbol{x})]\!])_{(\tilde{\Upsilon}^e)_n} \end{aligned} \tag{20}$$

where $(\mathcal{L}_1 w^h - f = \nabla^2 w^h - a^2 \ddot{w^h} - f)$ is the residual for the wave equation, $(\mathcal{L}_2 w^h = w^h_{,n} + \mathbb{S}_1 w^h)$ is the radiation boundary residual, and $(\mathcal{L}_3 w^h = w^h_{,n} - \dot{\boldsymbol{u}}\cdot\boldsymbol{n})$ is the interface boundary residual. In the above expressions, a tilde refers to integration over element interiors and τ and s are local mesh parameters designed to improve desirable high frequency numerical dissipation without degrading the accuracy of the underlying time-discontinuous Galerkin method. For the structural equation (8) similar least-squares terms are added, see [14, 15]. Consistency of both the underlying method and the least-squares addition is clear from the fact that a sufficiently smooth exact solution of the initial/boundary-value problem satisfies the variational equation (6) and (20) identically. Similar GLS methods have been used to enhance the stability and accuracy of solutions to the related reduced wave equation (Helmholtz equation) governing time-harmonic acoustics in the frequency domain, see [29, 30, 31].

7 Accuracy Analysis

Results are summarized from a convergence analysis of the space-time finite element formulation for the exterior structural acoustics problem. Results are also specialized

for a rigid scatterer. To study convergence, space-time mesh size parameters are introduced. For the fluid domain Ω_f, $h_f = \max\{c\Delta t\,,\,\Delta x\}$ where c is the acoustic wave speed and Δx and Δt are maximum element diameters in space and time, respectively. For a coupled elastic structure, $h_s = \max\{c_L\Delta t\,,\,\Delta x\}$ where c_L is the dilatational wave speed.

Assuming that the exact solution to the governing differential equations for structural acoustics with radiation boundary condition $\mathbb{S}_1$, is sufficiently smooth, and assuming standard finite element interpolation estimates hold, then it has been proved in [14] that the following error estimate holds for the time-discontinuous GLS formulation,

$$|||\boldsymbol{E}|||^2 \quad \leq \quad c(\boldsymbol{u})\, h_s^{2k-1} \,+\, c(\phi)\, h_f^{2p-1} \tag{21}$$

where k and p are the finite element interpolation orders for the structure and fluid respectively. In the above, the error is defined as

$$\boldsymbol{E} = \{\boldsymbol{e}\,,\,e\} \qquad \text{where} \qquad \boldsymbol{e} = \boldsymbol{u}^h - \boldsymbol{u} \quad \text{and} \quad e = \phi^h - \phi, \tag{22}$$

and $c(\boldsymbol{u})$ and $c(\phi)$ are values that are independent of the mesh size parameters h_s and h_f. The norm in which convergence is measured is given by,

$$\begin{aligned} |||\boldsymbol{E}|||^2 \quad &= \quad |||e|||_f^2 \,+\, |||\boldsymbol{e}|||_s^2 \\ &+ \quad \sum_{n=0}^{N-1} \Big\{ (\boldsymbol{\sigma}(\nabla \boldsymbol{e})\cdot\boldsymbol{n} - \rho_f \dot{e}\boldsymbol{n}\,,\, \rho_s^{-1}\boldsymbol{s}\boldsymbol{\sigma}(\nabla \boldsymbol{e})\cdot\boldsymbol{n} - \rho_f \dot{e}\boldsymbol{n})_{(\Upsilon_i)_n} \\ &+ \quad (\dot{\boldsymbol{e}}\cdot\boldsymbol{n} - e_{,n}\,,\, c^2 s\dot{\boldsymbol{e}}\cdot\boldsymbol{n} - e_{,n})_{(\Upsilon_i)_n} \Big\} \end{aligned} \tag{23}$$

$$
\begin{aligned}
|||e|||_f^2 \quad &= \quad \mathcal{E}_f(e(0^+)) + \sum_{n=1}^{N-1} \mathcal{E}_f([\![e(t_n)]\!]) + \mathcal{E}_f(e(T^-)) \\
&+ \quad \frac{1}{2R}||e(0^+)||_{\Gamma_\infty}^2 + \sum_{n=1}^{N-1} \frac{1}{2R}||[\![e(t_n)]\!]||_{\Gamma_\infty}^2 + \frac{1}{2R}||e(T^-)||_{\Gamma_\infty}^2 \\
&+ \quad \sum_{n=0}^{N-1} \frac{1}{c} \int_{t_n}^{t_{n+1}} (\dot{e}(t)\,,\, \dot{e}(t))_{\Gamma_\infty}\, dt \\
&+ \quad \sum_{n=0}^{N-1} \Big\{ ||c\tau^{1/2}\mathcal{L}_1 e||_{\tilde{Q}_n^f}^2 + ||cs^{1/2}\mathcal{L}_2 e||_{(\tilde{\Upsilon}_\infty)_n}^2 \\
&+ \quad ||cs^{1/2}[\![e_{,n}(\boldsymbol{x})]\!]||_{(\tilde{\Upsilon}_f)_n}^2 \Big\} \qquad (24) \\
|||\boldsymbol{e}|||_s^2 \quad &= \quad \mathcal{E}_s(\boldsymbol{e}(0^+)) + \sum_{n=1}^{N-1} \mathcal{E}_s([\![\boldsymbol{e}(t_n)]\!]) + \mathcal{E}_s(\boldsymbol{e}(T^-)) \\
&+ \quad \sum_{n=0}^{N-1} \Big\{ (\mathcal{L}_s \boldsymbol{e}\,,\, \rho_s^{-1}\boldsymbol{\tau}\mathcal{L}_s \boldsymbol{e})_{\tilde{Q}_n^s} \\
&+ \quad ([\![\boldsymbol{\sigma}(\nabla \boldsymbol{e})(\boldsymbol{x})]\!]\cdot \boldsymbol{n}\,,\, \rho_s^{-1}\boldsymbol{s}[\![\boldsymbol{\sigma}(\nabla \boldsymbol{e})(\boldsymbol{x})]\!]\cdot \boldsymbol{n})_{(\tilde{\Upsilon}_s)_n} \Big\} \qquad (25)
\end{aligned}
$$

In the above expression $\mathcal{L}_s \boldsymbol{u}^h$ is the residual for the structure. This norm emanates naturally from the coupled fluid-structure variational equation (6) together with the least-squares operators discussed in Section 6. The error estimate is optimal in the sense that the finite element error converges at the same rate as the interpolate. This result indicates that the error for the coupled system is controlled by the convergence rates in both the structure and the fluid. In other words, for an accurate solution to the coupled fluid-structure problem, discretizations for both the structural domain and the fluid domain must be adequately resolved. For a rigid scatterer, (21) specializes to

$$
|||e|||_f^2 \quad \leq \quad c(\phi)\, h_f^{2p-1} \qquad (26)
$$

8 High-order Accurate Radiation Boundary Conditions

For large-scale simulations the use of high-order accurate radiation boundary conditions is essential to allow the fluid truncation boundary to be placed close to the

scatterer and thereby minimizing the mesh and matrix problem size. Non-reflecting boundary conditions for both two- and three-dimensional applications have been proposed by several authors; complete surveys prior to 1991 can be found in [32] and [33]. Recently, there has been interest in transforming the frequency dependent Dirichlet-to-Neumann (DtN) non-reflecting boundary condition derived in [34], to equivalent time-dependent boundary conditions for direct transient analysis. The DtN map represents the exact impedance relation on a seperable truncation fluid boundary. Time-dependent non-reflecting boundary conditions based on the DtN map which match the first N spherical wave harmonics on a spherical boundary Γ_∞ have been derived recently in [14, 28] and [35]. In [14, 28], two alternative sequences of time-dependent non-reflecting boundary conditions have been obtained; the first involves time derivatives while retaining a spatial integral (local in time and nonlocal in space version), and the second involves both time and spatial derivatives (local in time and local in space version). Both versions start with the nonlocal DtN map in the frequency domain, followed by an inverse Fourier transform. Interestingly, in the second version, the first two operators in the sequence are identical to the first two boundary conditions in the well-known sequence derived by Bayliss and Turkel, [27], which are obtained by annilating high-order radial terms in a multipole expansion for outgoing waves. For higher-order boundary conditions in the sequence beyond second-order, however, the boundary conditions derived in [14, 28] differ from those in [27]. An alternative form of the localized DtN non-reflecting boundary condition, obtained directly in the time-domain, is presented in [35].

In this section, we briefly review the development of the localized version of the time-dependent DtN map first derived in [14], and examine the relationship of these local radiation boundary conditions to the well-known sequence of boundary conditions derived in [27]. Next, a direct implementation of the second-order boundary conditions in the sequence of Bayliss and Turkel, or equivalently the second-order operator in the localized time-dependent DtN map for the time-discontinuous space finite element method is presented.

The nonlocal DtN map is derived in the frequency domain starting with the reduced wave equation (Helmholtz equation) in the exterior domain Ω_∞. Assuming harmonic time dependence $e^{-i\omega t}$ where $\omega > 0$, the exterior problem in Ω_∞ is,

$$\nabla^2\phi + k^2\phi = 0 \qquad \text{in } \Omega_\infty \tag{27}$$

$$\phi = \bar{\phi} \qquad \text{on } \Gamma_\infty \tag{28}$$

$$\lim_{r\to\infty} r^{(n_{sd}-1)/2}\left(\frac{\partial\phi}{\partial r} - ik\phi\right) = 0 \tag{29}$$

where $k = \omega/c \geq 0$ is the acoustic wave number and $\bar{\phi}$ is the restriction of ϕ to the truncation boundary Γ_∞. Restricting the boundary Γ_∞ to be of separable geometry it is possible to express the general solution as an infinite series of wave harmonics, see e.g. [36]. For the simple case of a sphere of radius $r = R$, and $n_{sd} = 3$, the

outgoing solution can be expressed in terms of spherical harmonics as:

$$\phi(r,\theta,\varphi) = \sum_{n=0}^{\infty} \frac{h_n(kr)}{h_n(kR)} Y_n(\theta\,,\,\varphi) \qquad r \geq R \tag{30}$$

where

$$Y_n(\theta\,,\,\varphi) = \sum_{j=0}^{n}{}' P_n^j(\cos\varphi)(A_{nj}\cos j\theta + B_{nj}\sin j\theta) \tag{31}$$

are spherical surface harmonics of order n, with nonlocal coefficients

$$A_{nj} = \alpha_{nj}\int_{\Gamma_\infty} \bar{\phi}(\theta\,,\,\varphi)\, P_n^j(\cos\varphi)\, \cos j\theta\; d\Gamma \tag{32}$$

$$B_{nj} = \alpha_{nj}\int_{\Gamma_\infty} \bar{\phi}(\theta\,,\,\varphi)\, P_n^j(\cos\varphi)\, \sin j\theta\; d\Gamma \tag{33}$$

and

$$\alpha_{nj} = \frac{(2n+1)(n-j)!}{2\pi R^2(n+j)!} \tag{34}$$

In the above, $0 \leq \theta < 2\pi$ is the circumferential angle and $0 \leq \varphi < \pi$ is the polar angle for a spherical truncation boundary of radius $r = R$. The differential surface area is $d\Gamma = R^2 \sin\varphi d\theta d\varphi$, P_n^j are associated Legendre functions of the first kind, and h_n are spherical Hankel functions of the first kind of order n. The prime after the sum indicates that a factor of $1/2$ multiplies the term with $j = 0$. The solution $\phi(R\,,\,\theta\,,\,\varphi)$, restricted to the spherical boundary is given by $\bar{\phi}(\theta\,,\,\varphi)$.

The DtN map relating Dirchlet-to-Neumann data on Γ_∞ is obtained by differentiating (30) with respect to r evaluated at $r = R$, see [34]:

$$\frac{\partial\phi}{\partial n}(R,\theta,\varphi) = \sum_{n=0}^{\infty} z_n(kR)\, Y_n(\theta\,,\,\varphi) \tag{35}$$

with impedance coefficients,

$$z_n(kR) = \frac{kh_n'(kR)}{h_n(kR)} \tag{36}$$

The prime on h_n indicates differentiation with respect to its argument. The DtN operator (35) represents the exact impedance for the exterior acoustic fluid restricted to the artificial boundary. Furthermore, since (35) is an integral operator coupling all points on the artificial boundary Γ_∞, it is a spatially nonlocal boundary condition in the frequency domain.

In [14, 28] a local in time counterpart to the spatially nonlocal DtN map (35) is derived which matches the first N spherical wave harmonics in the outgoing solution (30) on Γ_∞. This sequence of boundary conditions retains the nonlocal spatial integral, yet replaces a time-convoluted DtN map with higher-order local time derivatives.

This form of time-dependent boundary conditions has the advantage that when implemented in the time-discontinuous finite element formulation, standard $C^0(\Gamma_\infty \times I_n)$ interpolation functions may be used for both the space and time variables.

An alternative version is obtained by first localizing the acoustic impedance relation (35) in the frequency domain, followed by an inverse Fourier transform. In [14, 28] it is shown that when the solution on the boundary Γ_∞ contains only a finite number of spherical harmonics, then such a transformation gives an exact time-dependent counterpart which is local in both $\boldsymbol{x}$ and t. This sequence of local boundary conditions is obtained by truncating the DtN map (35), so that the sum ranging over n extends over the finite range $n = 0, 1, \cdots N-1$. The development proceeds by recognizing that Y_n can be interpreted as eigenfunctions of the Laplace-Beltrami operator

$$\Delta_\Gamma := \frac{1}{\sin\varphi}\frac{\partial}{\partial\varphi}\left(\sin\varphi\frac{\partial}{\partial\varphi}\right) + \frac{1}{\sin^2\varphi}\frac{\partial^2}{\partial\theta^2} \tag{37}$$

with eigenvalues $\lambda = -n(n+1)$, so that

$$[n(n+1)]^m Y_n = (-\Delta_\Gamma)^m Y_n \tag{38}$$

This property of the spherical harmonics suggests writing the impedance coefficients as a series of powers of $n(n+1)$, see [37] and [38]:

$$z_n(kR) = \sum_{m=0}^{N-1}[n(n+1)]^m \beta_m(kR), \qquad n = 0, 1, \cdots, N-1 \tag{39}$$

This system of N linear equations can be solved for the N unknown values $\beta_m, m = 0, 1, \cdots N$. By replacing z_n in the truncated series representation of (35) with (39), replacing $[n(n+1)]^m Y_n$ with the high-order tangential derivatives $(-\Delta_\Gamma)^m Y_n$, and using the assumption that the solution $\bar{\phi}$ on Γ_∞ contains only the first N spherical harmonics, the following sequence of local radiation boundary conditions is obtained:

$$\frac{\partial\phi}{\partial n} \quad = \quad \sum_{m=0}^{N-1}\beta_m(kR)\,(-\Delta_\Gamma)^m\phi \qquad \text{on} \;\; \Gamma_\infty \tag{40}$$

Since this sequence follows directly from the truncated DtN map, these radiation boundary operators annilate the first N spherical wave harmonics for the outgoing solution (30) on a spherical boundary Γ_∞.

Local time-dependent counterparts to (40) can be obtained by using the finite series expansion for the spherical Hankel functions

$$h_n(kr) = h_0(kr)\left[(-i)^n\sum_{j=0}^{n}\frac{(n+j)!}{j!(n-j)!}\left(\frac{-1}{2ikr}\right)^j\right], \quad n = 0, 1, 2, \cdots \tag{41}$$

evaluated at $r = R$ which are embedded in $\beta_m(kR)$, and then taking an inverse Fourier transform.

For example, for $N = 2$, the system (39) can be solved to obtain $\beta_0 = z_0$ and $\beta_1 = (z_1 - z_0)/2$. Using this result in the local DtN condition (40) gives,

$$\frac{\partial \phi}{\partial n} = z_0 \phi + \frac{1}{2}(z_0 - z_1)\Delta_\Gamma \phi \tag{42}$$

Clearing the common denominator $h_0 h_1$ and using the recurrence relation

$$h_n' = h_{n-1} - \left(\frac{n+1}{kR}\right) h_n \,, \qquad n = 1, 2, \cdots \tag{43}$$

in conjunction with (41) leads to,

$$\left(\frac{1}{R} - ik\right)\frac{\partial \phi}{\partial n} \quad = \quad \left(k^2 + \frac{2ik}{R} - \frac{1}{R^2}\right)\phi + \frac{1}{2R^2}\Delta_\Gamma \phi \tag{44}$$

Since this expression involves only terms in powers of (ik), an inverse Fourier transform is readily obtained with the result,

$$\mathbb{B}_2 \phi := \frac{\partial \phi}{\partial n} + \frac{R}{c}\frac{\partial \dot{\phi}}{\partial n} + \frac{R}{c^2}\ddot{\phi} + \frac{2}{c}\dot{\phi} + \frac{1}{R}\phi - \frac{1}{2R}\Delta_\Gamma \phi = 0 \tag{45}$$

When applied on a spherical boundary Γ_∞, this operator acts as a higher-order accurate local boundary condition which is perfectly absorbing for the first two spherical wave harmonics of orders $n = 0$ and $n = 1$. As the order N is increased, i.e. more terms are used in (40), the resulting boundary conditions $\mathbb{B}_N \phi$ match more terms in the harmonic expansion for outgoing waves, and a better approximation is obtained: see [14, 28] for expressions for the time-dependent counterparts to (40) for $N \geq 3$.

For the simple case $N = 1$, the boundary condition resulting from the time-dependent counterpart to (40) is equivalent to the 'spherical damper' expressed in (5), as expected! It should also be noted that the first-order boundary condition in the sequences derived by Engquist and Majda, [39, 40], and Bayliss and Turkel, [27], also coincide with the well-known 'spherical damper' boundary condition. Furthermore, for the case $N = 2$, the time-dependent counterpart to the localized DtN operator (40), i.e. the operator $\mathbb{B}_2$ defined in (45), is identical to the second-order radiation boundary condition derived by Bayliss and Turkel in [27], after second-order radial derivatives are eliminated in favor of second-order tangential derivatives through use of the wave equation in spherical coordinates. Thus, while the boundary conditions derived by Bayliss and Turkel were obtained by annilating radial terms in a multipole expansion, it is seen, that in fact, the first two boundary conditions in the sequence share the property of the localized DtN, in that they match the first two spherical harmonics for outgoing waves on a spherical boundary Γ_∞. For higher-order boundary conditions in the sequence beyond $N \geq 3$, the form of the boundary conditions derived in [14, 28] differ from those derived in [27]. Both sequences of local time-dependent boundary conditions provide increasing accuracy with order N, which, however, is also a measure of the difficulty of implementation.

For the localized DtN, the Nth-order condition contains all the even tangential and temporal derivatives up to order $2(N-1)$, while in the sequence of Bayliss and Turkel, the Nth-order condition contains all even tangential derivatives up to order N, for $N = 2, 4, 6, \cdots$, and up to order $N-1$, for $N = 3, 5, \cdots$. The number of temporal derivatives appearing in the sequence [27] is equivalent to [28]. Because the time-discontinuous formulation allows for the use of $C^0(\Gamma_\infty \times I_n)$ interpolations to represent the high-order time derivatives, it is possible to implement these sequences of time-dependent absorbing boundary conditions up to any order desired. However for higher-order operators extending beyond $N \geq 3$, the lowest possible order of spatial continuity on the artificial boundary that can be achieved after integration by parts is C^{N-2}. For these high-order operators a layer of boundary elements adjacent to Γ_∞, possessing high-order tangential continuity on Γ_∞ are needed, see e.g. [41].

8.1 Space-Time Finite Element Implementation

A direct approach for implementing time-dependent radiation boundary conditions is to define a linear operator $\mathbb{S}_N$ such that,

$$\mathbb{B}_N(\phi) := \frac{\partial \phi}{\partial n} + \mathbb{S}_N(\phi) \tag{46}$$

which implies

$$\nabla\phi \cdot \boldsymbol{n} \quad = \quad -\mathbb{S}_N\phi \qquad \text{on} \;\; \Upsilon_\infty \equiv \Gamma_\infty \times I \tag{47}$$

In this way, the boundary conditions are expressed in a form relating Dirchlet-to-Neumann data and can be incorporated into the Galerkin variational equation as natural boundary conditions: for the case of the space-time finite element method, the boundary conditions are weakly enforced in both space and time; for the case of the standard semidiscrete finite element method, the boundary conditions are weakly enforced in space, and then integrated in time using standard finite difference schemes.

For example, for $N = 2$;

$$\mathbb{S}_2\phi = \frac{1}{2R}(2 - \Delta_\Gamma)\phi + \frac{1}{c}\left(2 + R\frac{\partial}{\partial r}\right)\phi_{,t} + \frac{R}{c^2}\phi_{,tt} \tag{48}$$

In the time-discontinuous Galerkin formulation, the operator defined on Γ_∞ in Eq. (7) takes the form:

$$\begin{aligned} G_\infty(w^h\,,\,\phi^h)_n \quad &= \quad \int_{t_n}^{t_{n+1}} (\dot{w}^h\,,\,\mathbb{S}_2\phi^h)_{\Gamma_\infty}\; dt \\ &+ \quad d_2\big(\dot{w}^h(t_n^+)\,,\,[\![\dot{\phi}^h(t_n)]\!]\big)_{\Gamma_\infty} \;+\; d_0\big(w^h(t_n^+)\,,\,[\![\phi^h(t_n)]\!]\big)_{\Gamma_\infty} \end{aligned} \tag{49}$$

where

$$\int_{t_n}^{t_{n+1}} \left(\dot{w}^h\,,\,\mathbb{S}_2\phi^h\right)_{\Gamma_\infty} dt \quad = \quad d_0\left(\dot{w}^h\,,\,\phi^h\right)_{(\Upsilon_\infty)_n} + d_1\left(\dot{w}^h\,,\,\dot{\phi}^h\right)_{(\Upsilon_\infty)_n} + d_2\left(\dot{w}^h\,,\,\ddot{\phi}^h\right)_{(\Upsilon_\infty)_n} \tag{50}$$

and

$$\begin{aligned} d_0\left(\dot{w}^h\,,\,\phi^h\right)_{(\Upsilon_\infty)_n} &= \frac{\rho_f}{R}\int_{t_n}^{t_{n+1}} (\dot{w}^h\,,\,\phi^h)_{\Gamma_\infty}\,dt + \frac{\rho_f}{2R}\int_{t_n}^{t_{n+1}} (\dot{w}^h_{,\varphi}\,,\,\phi^h_{,\varphi})_{\Gamma_\infty}\,dt \\ &+ \frac{\rho_f}{2R}\int_{t_n}^{t_{n+1}} (\dot{w}^h_{,\theta}\,,\,\csc^2(\varphi)\,\phi^h_{,\theta})_{\Gamma_\infty}\,dt \end{aligned} \tag{51}$$

$$d_1\left(\dot{w}^h\,,\,\dot{\phi}^h\right)_{(\Upsilon_\infty)_n} = \frac{2\rho_f}{c}\int_{t_n}^{t_{n+1}} (\dot{w}^h\,,\,\dot{\phi}^h)_{\Gamma_\infty}\,dt + \frac{\rho_f R}{c}\int_{t_n}^{t_{n+1}} (\dot{w}^h\,,\,\dot{\phi}^h{}_{,r})_{\Gamma_\infty}\,dt \tag{52}$$

$$d_2\left(\dot{w}^h\,,\,\ddot{\phi}^h\right)_{(\Upsilon_\infty)_n} = \frac{\rho_f R}{c^2}\int_{t_n}^{t_{n+1}} (\dot{w}^h\,,\,\ddot{\phi}^h)_{\Gamma_\infty}\,dt \tag{53}$$

In (51), continuity requirements due to second-order tangential derivatives in the Laplace-Beltrami operator Δ_Γ, are relaxed on the artificial boundary Γ_∞, through integration by parts.

The form of the terms defined in (49) involving temporal jump operators $[\![\cdot]\!]$, evaluated on the boundary Γ_∞, can be inferred from equations (51) and (53). These consistent jump terms act to weakly enforce continuity of $\phi^h(t_n)$ and $\dot{\phi}^h(t_n)$ between space-time-slabs at the boundary Γ_∞. These additional operators are needed in order to ensure unconditional stability for the time-discontinuous Galerkin space time finite element method; see [28] for an example illustrating an instability in the time-discontinuous Galerkin solution resulting from the omission of these jump operators on Γ_∞.

The direct implementation of (45) in a stable semidiscrete finite element formulation for the coupled structural acoustics problem in exterior domains is given in [7, 8, 33]. The second-order boundary condition can also be implemented indirectly through the addition of auxillary variables resulting in a spatially symmetric boundary operator [42]; see [11] for application of this indirect approach in the standard semidiscrete finite element method for two-dimensional analysis using the classical trapezoidal rule for integrating in time; see also [28] for a discussion of this approach for implementation in the space-time finite element method.

9 Representative Numerical Examples

Numerical examples are presented to demonstrate the effectiveness of the time-discontinuous Galerkin space-time finite element method to accurately model transient radiation and scattering from geometrically complex surfaces. The problems investigated also

assesses the performance of the first- and second-order local radiation boundary conditions through a direct implementation in the space-time finite element formulation. For the numerical results presented, the structure is assumed rigid, i.e. $c_L/c = \infty$, the GLS mesh parameters are set to zero and C^0 quadratic shape functions (Lagrange interpolation) are used in isoparametric space-time finite elements.

9.1 Nonconcentric spherical radiator

To illustrate the improved accuracy that can be obtained by using high-order radiation boundary conditions, we consider a sphere of radius $r = a$, pulsating with a uniform sine pulse, $\phi(a,t) = \sin\omega t$ and $\omega = \pi$, during the short time interval $t \in [0,1]$. Comparisons are made with the first-order $\mathbb{S}_1$, and second-order $\mathbb{S}_2$, local boundary conditions defined in (5) and (48) respectively. Initial conditions are set to zero and the wave speed is $c = 1$. The exact solution to this problem is an outgoing spherical wave of short duration with a $1/r$ amplitude decay:

$$\phi(r\,,\,t) \quad = \quad \left(\frac{a}{r}\right)\sin\omega(t - \bar{r}/c) \tag{54}$$

where $\bar{r} = r - a$ is the radial distance from the spherical radiator and $(t - \bar{r}/c) \in [0,1]$.

If the radiating sphere is placed concentric with a spherical artificial boundary, then for the uniform radiation field given in (54), the problem is trivial in that the first order $\mathbb{S}_1$, and higher order local non-reflecting boundary conditions are all exact by design, i.e. the localized DtN boundary conditions all match the first $n = 0$, spherical harmonic. In order to obtain a challenging problem, the radiating sphere is shifted from the center of the spherical artificial boundary Γ_∞, to a nonconcentric position. In this example, the radiating sphere is offset by a distance a, with the radius of Γ_∞ set at $R = 3a$, see Figure 3. With this positioning, wave fronts traveling outward along radial lines will strike the artificial boundary at oblique angles. The closer the radiating sphere gets to the edge of Γ_∞, the more acute this angle becomes, making it increasingly difficult for the local boundary conditions to transmit outgoing waves without spurious reflection.

Figure 3 shows the computational domain discretized with 1518 axisymmetric elements using quadratic interpolation. As a consequence of the axisymmetric nature of the problem, there is no circumferential dependence on the solution and all terms which depend on the coordinate θ are neglected in the definition of the non-reflecting boundary conditions. In particular, for the local boundary operator $\mathbb{S}_2$ defined in (48), the terms involving derivatives of θ in (51) and (53) are neglected.

Figure 4 shows the contours of the time-discontinuous Galerkin solution using the second-order local boundary operator $\mathbb{S}_2$ defined in (48) applied to Γ_∞. As time progresses, the initial pulse propagates outward from the sphere as a uniform spherical wave of decreasing amplitude. The numerical simulation is continued until just prior to reaching the disappearance of the pulse from the computational domain. After $t = 1$, the spherical pulse begins to pass through the artificial boundary Γ_∞ with no

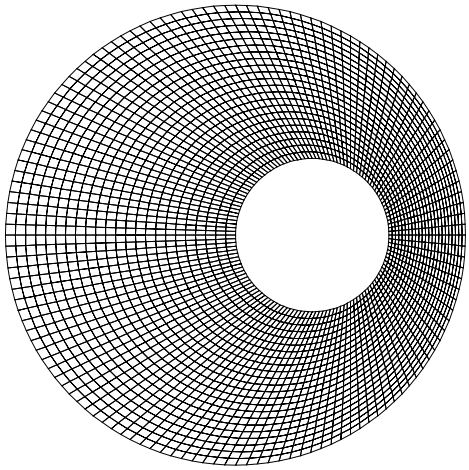

Fig. 3: Computational domain for a sphere of radius a, offset from the center of a spherical non-reflecting boundary of radius $3a$. Illustration of spatial discretization: Upper half modeled with 1518 axisymmetric space-time elements using piecewise polynomial quadratic interpolation.

observable reflection, as manifested by the negligible wake (clear blue area) behind the wavefront. This result illustrates the ability of the second-order operator $\mathbb{S}_2$ to transmit waves striking the artificial boundary at rather severe angles.

For comparison, this same problem was solved with the first-order boundary operator $\mathbb{S}_1$ defined in (5). Figure 5 shows the solution contours using $\mathbb{S}_1$. These results illustrate that the solution using $\mathbb{S}_1$ exhibits significant reflections as the outgoing pulse passes through Γ_∞, as indicated by the dark blue contours appearing in the solution. This conclusion is summarized in Figure 6 as a time history of the solution on the artificial boundary Γ_∞ at the axis of symmetry. The solution using the second-order operator $\mathbb{S}_2$ shows the correct amplitude and phase for the outgoing pulse, and shows no observable reflections behind the wave front. In contrast, the solution using the first-order operator $\mathbb{S}_1$ shows the incorrect maximum amplitude of the outgoing pulse as well as significant reflections, as manifested by the non-zero amplitudes appearing for times $t > 2$. This example illustrates the importance of using a high-order accurate non-reflecting boundary condition for numerical solution of the exterior acoustics problem.

9.2 Transient scattering from an infinite cylinder

In this example we consider the simulation of transient scattering from an infinite rigid cylinder with conical-to-spherical ends and a large length to width ratio, $L/d = 6.1$. Figure 7 illustrates the finite element spatial discretization of the computational domain. A total of 1600 space-time quadratic elements are used for this example. For this problem, the local radiation boundary conditions defined in two spatial dimen-

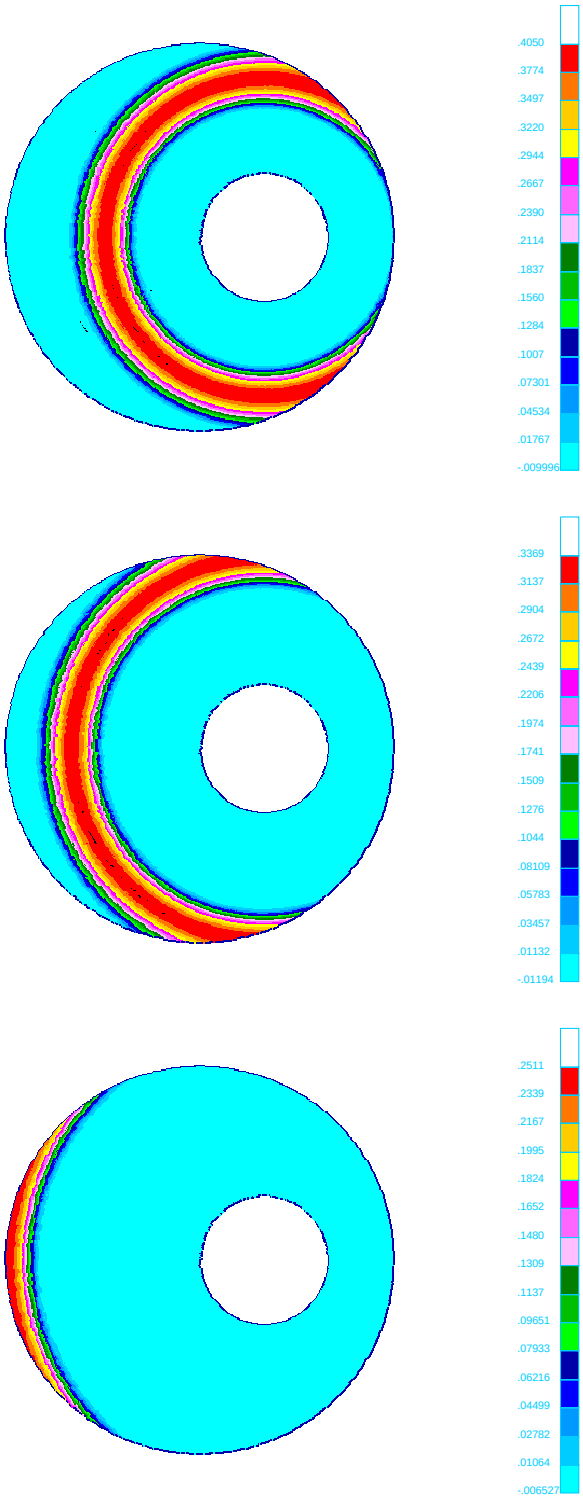

Fig. 4: Radiation from a nonconcentric sphere. Results obtained using the local second-order radiation boundary condition $\mathbb{S}_2$. Solution contours shown at times $t = 2.0, 2.5$ and $t = 3.5$

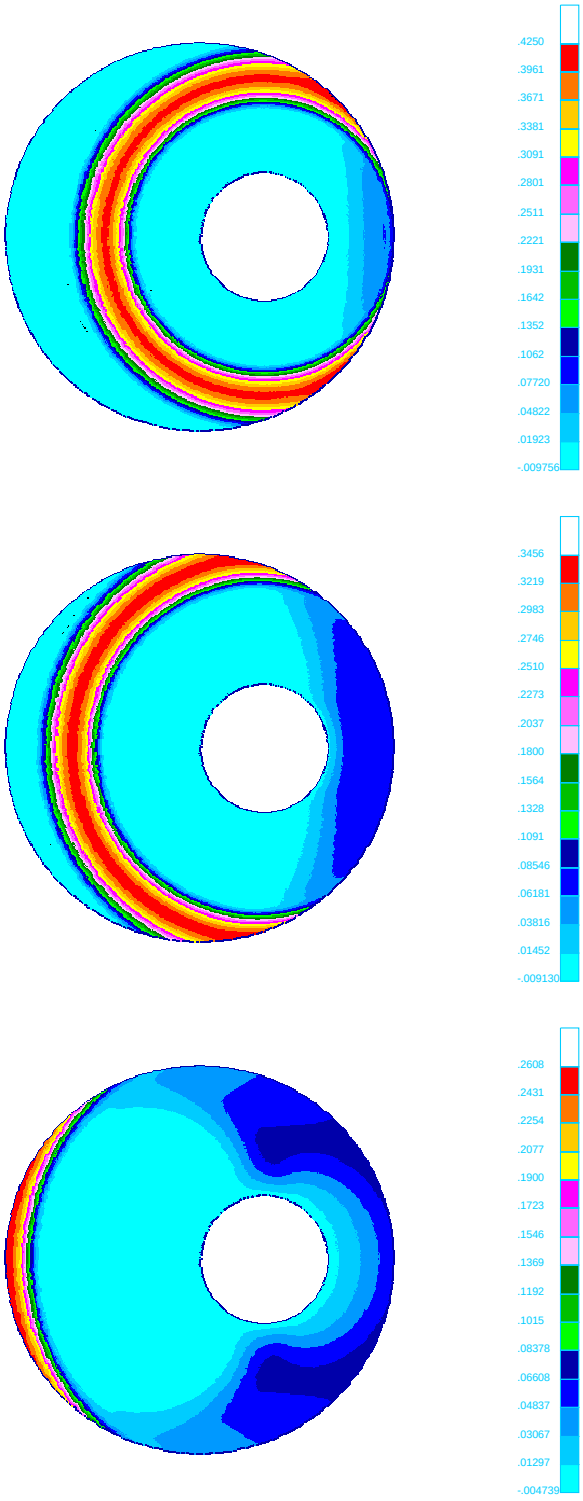

Fig. 5: Radiation from a nonconcentric sphere. Results obtained using the local first-order radiation boundary condition $\mathbb{S}_1$. Solution contours shown at times $t = 2.0, 2.5$ and $t = 3.5$

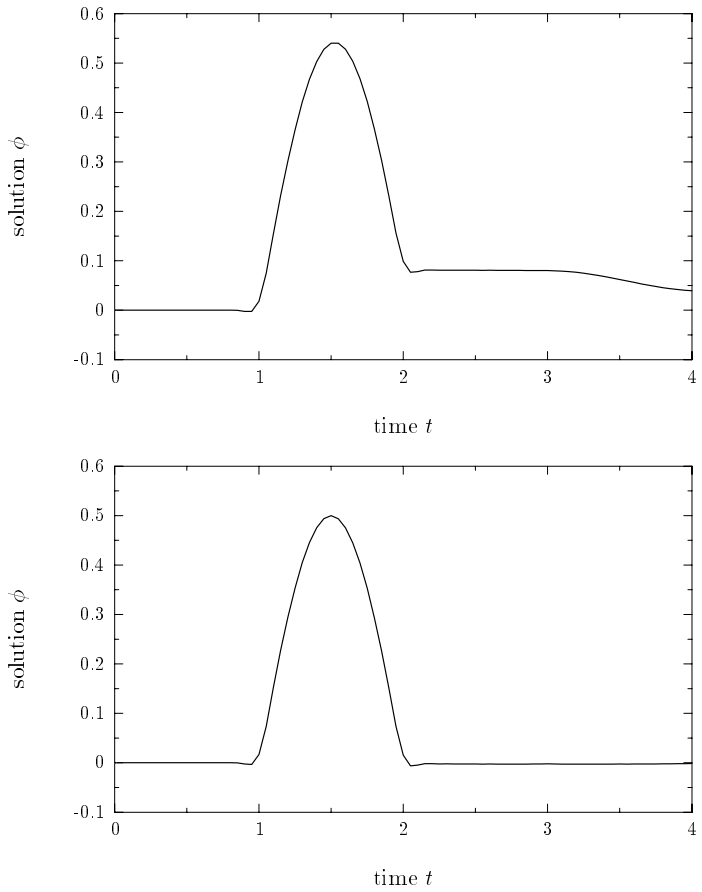

Fig. 6: Radiation from a nonconcentric sphere: Solution on the artificial boundary Γ_∞, at the axis of symmetry $\varphi = 0$. (top) $\mathbb{S}_1$ local boundary condition. (bottom) $\mathbb{S}_2$ local boundary condition.

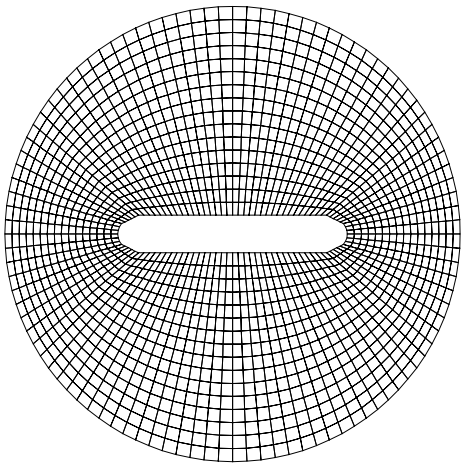

Fig. 7: Spatial discretization for cylinder with conical to spherical ends. (1600 quadratic elements)

sions described in [43, 10] are used. In particular, the following second-order local time-dependent boundary operator is applied on a circular boundary Γ_∞,

$$S_2\phi = \frac{1}{2R}(3/4 - \frac{\partial^2}{\partial\theta^2})\phi + \frac{3}{2c}\dot{\phi} + \frac{R}{c}\frac{\partial\dot{\phi}}{\partial r} + \frac{R}{c^2}\ddot{\phi} \tag{55}$$

The direct implementation of (55) in the time-discontinuous Galerkin space-time formulation through the operator G_∞, takes on a similar form to the expression for the $\mathbb{S}_2$ operator (48) defined in three space dimensions, and implemented in (49); further details are given in [26].

The driver for this problem is the source $f = \delta(x_0, y_0)\sin\omega t$ for the time interval $t \in [0, 3]$, positioned inside the computational domain such that an incident wave strikes the scatterer at an oblique angle. The phase speed is set at $c = 1$ with frequency $\omega = \pi/3$. To simulate an infinite structural impedance on Γ_i, homogeneous Neumann boundary conditions, i.e. 'rigid' boundary conditions, are prescribed on the cylinder surface. This example represents a challenging problem where the multiple-scales involving the ratio of the wavelength to diameter and length dimension play a critical role in the complexity of the resulting scattered wave field.

The numerical simulation at the end of the initial pulse at $t = 3$ is shown at the top of Figure 8. The subsequent illustrations in Figure 8 and Figure 9 show the contours of the scattering phenomena as time progresses. The solution is presented in terms of the scalar velocity potential ϕ: Results for other solution variables such as the acoustic pressure $p = -\rho_0\dot{\phi}$, or the acoustic velocity vector $\boldsymbol{v} = \nabla\phi$, are obtained through simple calculations of the time derivative and gradient of the velocity potential. The following sequence of events occur:

- At $t = 6$ the incident pulse has expanded in a cylindrical wave and has just

reached the surface of the rigid cylinder, while at the artificial boundary, the wave front passes through the boundary with negligible reflection.

- At $t = 9$ through $t = 12$, the incident wave has begun to reflect off the cylinder boundary, creating a complicated backscattered wave. The amplitude of the backscattered wave is positive creating a high intensity zone near the rigid structure in areas where the incident and backscattered waves coincide.

- At $t = 15$, the incident wave begins to scatter into a part that travels along the upper part of the cylinder, and a part that diffracts around the backside. The backscattered wave is seen to transmit through the radiation boundary with no observable reflection.

- At $t = 18$, the incident wave has passed over the cylinder and continues to be absorbed through the non-reflecting boundary. A quiescent state near the right of the cylinder suggests the effectiveness of the local boundary condition in absorbing outgoing waves.

10 Conclusions

In this paper, a stable and high-order accurate space-time finite element method for solution of the transient acoustics problem in exterior domains has been presented. The formulation is based on the time-discontinuous Galerkin method for general second-order hyperbolic systems developed by Hughes and Hulbert [12] in the context of elastodynamics, and incorporates a time-discontinuous implementation of the local second-order radiation boundary condition derived by Bayliss and Turkel [27], which is shown to be identical to the second-order operator in a localized version of the time-dependent Dirichlet-to-Neumann (DtN) map derived in [14, 28]. While the Bayliss and Turkel operator is obtained from annilating second-order radial derivatives in a multipole expansion, the operator shares an important property of the second-order operator in the truncated DtN map; namely, it matches the first two spherical harmonics for outgoing waves on a spherical radiation boundary. This observation plays an important role in the understanding of how individual wave harmonics contribute to the accuracy and stability of the solution as effected by the radial distance of the artificial boundary from the source, the geometric complexity of the wave pattern, and the frequency content for outgoing waves; see [28]. As the order of these and other non-reflecting boundary conditions increases they become increasingly difficult to implement in standard time-domain solution methods, e.g. semi-discrete methods, due to the occurrence of high-order time derivatives on the fluid truncation boundary. The time-discontinuous Galerkin space-time method provides a natural variational setting for the incorporation of general high-order accurate non-reflecting boundary conditions possessing the property of being local in

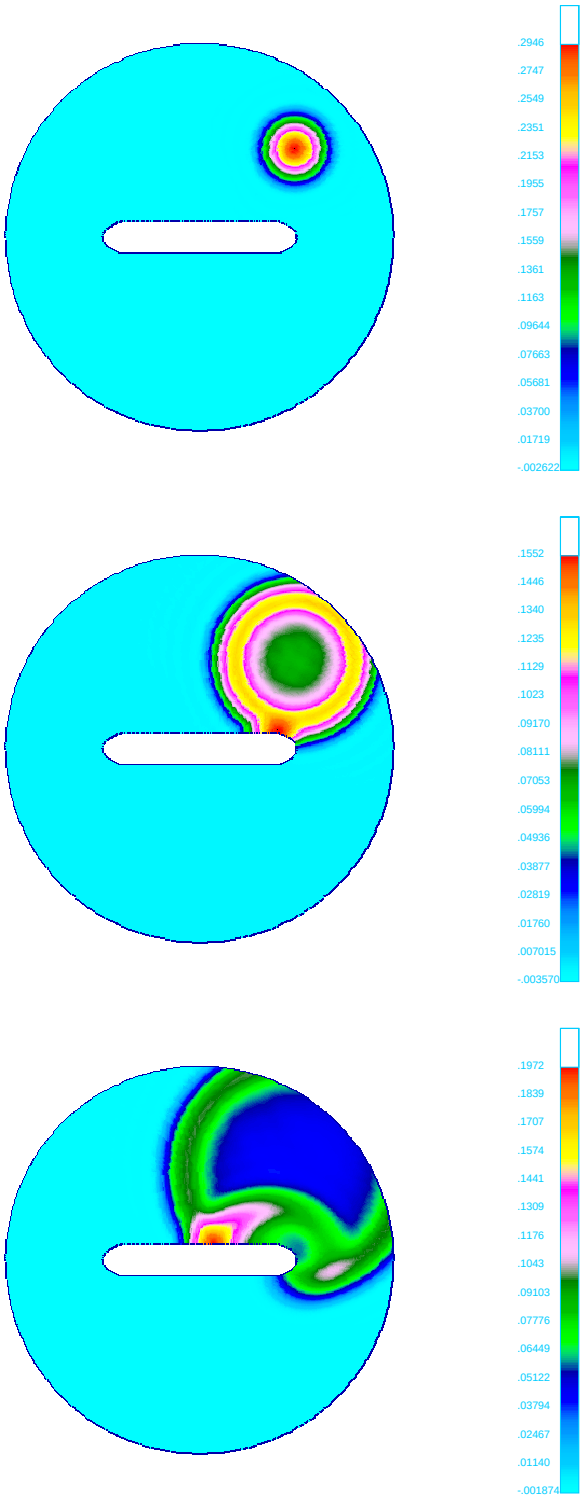

Fig. 8: Scattering from a 'rigid' cylinder with tapered ends due to a time-dependent point source. Solution contours shown at the end of the initial pulse at $t = 3$ and later times $t = 6$ and $t = 9$.

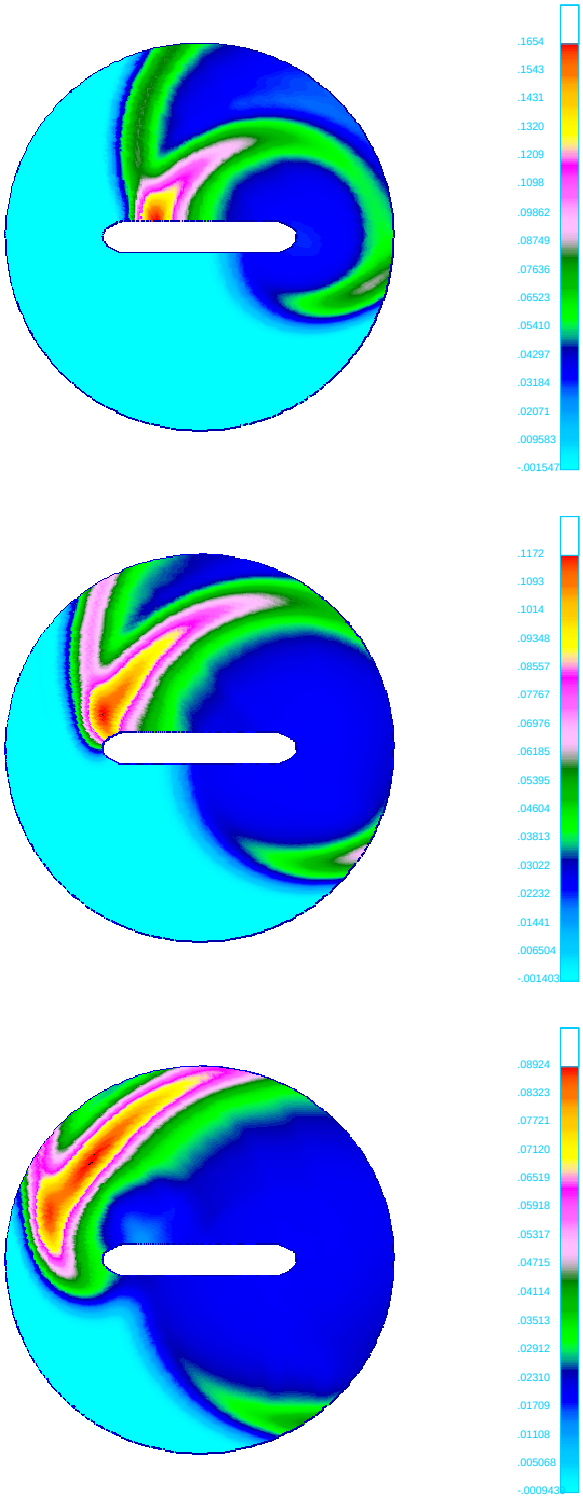

Fig. 9: Scattering from a 'rigid' cylinder with tapered ends due to a time-dependent point source. Solution contours shown at times $t = 12, 15, 18$.

time. This is accomplished in the time-discontinuous formulation by allowing for the use of C^0 continuous finite element basis functions in time. Crucial to the unconditional stability and optimal convergence rates of the time-discontinuous Galerkin formulation is the introduction of consistent temporal jump operators across space-time slabs restricted to the radiation boundary. The specific form of these operators are designed such that continuity of the solution across slabs is weakly enforced in a form consistent with the absorbing boundary conditions.

The resulting space-time algorithm gives for the first time a general solution to the fundamental problem of constructing a finite element method for the exterior acoustics problem with unstructured meshes in space-time and with the desired combination of good stability and high accuracy. Desirable attributes of this computational approach for transient acoustics include a natural framework for the design of rigorous *a posteriori* error estimates for self-adaptive solution strategies for unstructured space-time discretizations, and the implementation of high-order accurate time-dependent non-reflecting boundary conditions. Results from a functional analysis of the formulation indicates that the method is unconditionally stable, i.e, in the absense of any sources, the acoustic energy at any time t, plus the energy absorbed through the radiation boundary, is always less than, or equal to the initial energy in the system. High-order accuracy is obtained simply by raising the order of the space-time polynomial basis functions; both standard nodal interpolation and hierarchical shape functions are accommodated.

Numerical solutions obtained for the time-dependent acoustic radiation from a nonconcentric sphere demonstrated the excellent agreement between the exact and approximate solution using a direct implementation of high-order accurate non-reflecting boundary conditions in the space-time variational formulation. In particular, results confirm the superiority of the second-order local non-reflecting boundary condition $\mathbb{S}_2$ defined in (48), in comparison to the first-order $\mathbb{S}_1$ boundary condition defined in (5). It has also been demonstrated that with proper usage, the second-order non-reflecting boundary condition, when implemented in the space-time finite element method, is sufficiently accurate to capture the important physics associated with a complicated transient scattering problem involving some rather severe geometric and time scales. Additional numerical examples for transient wave propagation in three- and two- space dimensions are reported in [28] and [26], respectively.

In this paper we have concentrated on the accuracy of the solution for the uncoupled fluid. However, the present formulation for the exterior fluid is readily extended to the coupled fluid-structure interaction problem involving complex submerged structures. By using the acoustic velocity potential as the solution variable for the fluid, together with structural displacements as the solution variables for an elastic solid, the time-discontinuous method is proven in [14] to be unconditionally stable and to converge at an optimal rate for the structural acoustics problem; further details on the formulation, stability, and convergence of this space-time finite element method for structural acoustics in infinite domains are reported in [14, 15, 28, 26]. Further-

more, the extension to a multi-field formulation, where independent finite element approximations are used for the structural displacement vector and its time derivative, together with independent approximations for the acoustic pressure and velocity potential has recently been developed in [44].

Acknowledgments

This research was supported by the U.S. Office of Naval Research under grants N00014-89-J-1951 and N00014-92-J-1774. The first author was also supported by an Achievement Rewards for College Scientists (ARCS) fellowship. This support is gratefully acknowledged. The authors also express their appreciation to the anonymous reviewer for comments on this manuscript.

References

[1] W.J. Mansur and C.A. Brebbia. Formulation of the boundary element method for transient problems governed by the scalar wave equation. *Appl. Math. Modelling*, 6:307–311, 1982.

[2] W.J. Mansur and C.A. Brebbia. Further developments on the solution of the transient scalar wave equation. In C.A. Brebbia, editor, *Topics in Boundary Element Research*, volume 2, Berlin, 1984. Springer-Verlag.

[3] H. Huang, G.C. Everstine, and Y.F. Wang. Retarded potential techniques for the analysis of submerged structures impinged by weak shock waves. In T. Belytschko and T.L. Geers, editors, *Computational Methods for Fluid-Structure Interaction Problems*, volume AMD 26, pages 83–93. ASME, 1977.

[4] H.C. Neilson, G.C. Everstine, and Y.F. Wang. Transient response of a submerged fluid-coupled double-walled shell structure to a pressure pulse. *J. Acoust. Soc. Am.*, 70(6):1776–1782, 1981.

[5] Y.P. Lu. The application of retarded potential techniques to submerged dynamic structural systems. In R.P. Shaw and W. Pilkey, editors, *Proceedings of the 2nd Int. Symposium Innovative Numerical Analysis for the Applied Enginneering Sciences*, pages 59–68, 1980.

[6] A. Safjan, L. Demkowicz, and J.T. Oden. Adaptive finite element methods for hyperbolic systems with application to transient acoustics. *Int. J. Numer. Methods Engng.*, 32:677–707, 1991.

[7] P.M Pinsky and N.N. Abboud. Transient finite element analysis of the exterior structural acoustics problem. *ASME J. Vibration and Acoustics*, 112(2):245–256, 1990.

[8] P.M Pinsky and N.N. Abboud. Finite element solution of the transient exterior structural acoustics problem based on the use of radially asymptotic boundary operators. *Comp. Methods in Applied Mech. Engng.*, 85:311–348, 1991.

[9] P.M. Pinsky and L.L. Thompson. Accuracy of local non-reflecting boundary conditions for time-dependent structural acoustics. In *Structural Acoustics*, volume NCA-12/AMD-128, pages 153–160. ASME, 1991.

[10] P.M. Pinsky, L.L. Thompson, and N.N. Abboud. Local high order radiation boundary conditions for the two-dimensional time-dependent structural acoustics problem. *J. Acoust. Soc. Am.*, 91(3):1320–1335, 1992.

[11] L.F. Kallivokas and J. Bielak. Time-domain analysis of transient structural acoustics problems based on the finite element method and a novel absorbing boundary element. *J. Acoust. Soc. Am.*, 94(6):3480–3492, 1993.

[12] T.J.R. Hughes and G.M. Hulbert. Space-time finite element methods for elastodymamics: Formulations and error estimates. *Comp. Methods in Applied Mech. Engng.*, 66:339–363, 1988.

[13] G.M. Hulbert and T.J.R. Hughes. Space-time finite element methods for second-order hyperbolic equations. *Comp. Methods in Applied Mech. Engng.*, 84:327–348, 1990.

[14] L.L. Thompson. *Design and Analysis of Space-time and Galerkin Least-Squares Finite Element Methods for Fluid-Structure Interaction in Exterior Domains.* PhD thesis, Stanford University, April 1994.

[15] L.L. Thompson and P.M. Pinsky. A space-time finite element method for structural acoustics in infinite domains, Part I: Formulation, stability, and convergence. *Comp. Methods in Applied Mech. Engng.*, 132:195–227, 1996.

[16] C. Johnson. Discontinuous Galerkin finite element methods for second order hyperbolic problems. *Comp. Methods in Applied Mech. Engng.*, 107:117–129, 1993.

[17] P. Lesaint and P.A. Raviart. On a finite element method for solving the neutron transport equation. In C. de Boor, editor, *Mathematical Aspects of Finite Elements in Partial Differential Equations*, pages 89–123, New York, 1974. Academic Press.

[18] C. Johnson, U. Navert, and J. Pitkaranta. Finite element methods for linear hyperbolic problems. *Comp. Methods in Applied Mech. Engng.*, 45:285–312, 1984.

[19] C. Johnson. *Numerical Solutions of Partial Differential Equations by the Finite Element Method.* Cambridge University Press, 1986.

[20] T.J.R. Hughes. Recent progress in the development and understanding of SUPG methods with special reference to the compressible Euler and Navier-Stokes equations. *Int. J. Numer. Methods Engng.*, 7:1261–1275, 1987.

[21] F. Shakib. *Finite element analysis of the compressible Euler and Navier-Stokes equations*. PhD thesis, Stanford University, 1988.

[22] F. Shakib, T.J.R. Hughes, and Z. Johan. A new finite element formulation for computational fluid dynamics, X: The compressible Euler and Navier-Stokes equations. *Comp. Methods in Applied Mech. Engng.*, 89:141–219, 1991.

[23] G. Hauke and T.J.R. Hughes. A unified approach to compressible and incompressible flows. *Comp. Methods in Applied Mech. Engng.*, 113:389–395, 1994.

[24] T.J.R. Hughes, L.P. Franca, and G.M. Hulbert. A new finite element formulation for computational fluid dynamics: VIII. the Galerkin/least-squares method for advective-diffusive equations. *Comp. Methods in Applied Mech. Engng.*, 73:173–189, 1989.

[25] K. Jansen, Z. Johan, and T.J.R. Hughes. Implementation of a one-equation turbulence model within a stabilized finite element formulation of a symmetric advective-diffusive system. *Comp. Methods in Applied Mech. Engng.*, 105:405–433, 1993.

[26] L.L. Thompson and P.M. Pinsky. A space-time finite element method for the exterior structural acoustics problem: Time-dependent radiation boundary conditions in two spatial dimensions. *Int. J. Numer. Methods Engng.*, 39:1635–1657, 1996.

[27] A. Bayliss and E. Turkel. Radiation boundary conditions for wave-like equations. *Commun. Pure Appl. Math.*, 33:707–725, 1980.

[28] L.L. Thompson and P.M. Pinsky. A space-time finite element method for structural acoustics in infinite domains, Part II: Exact time-dependent non-reflecting boundary conditions. *Comp. Methods in Applied Mech. Engng.*, 132:229–258, 1996.

[29] I. Harari and T.J.R. Hughes. Finite element methods for the Helmholtz equation in an exterior domain: Model problems. *Comp. Methods in Applied Mech. Engng.*, 87:59–96, 1991.

[30] I. Harari and T.J.R. Hughes. Galerkin/least-squares finite element methods for the reduced wave equation with non-reflecting boundary conditions in unbounded domains. *Comp. Methods in Applied Mech. Engng.*, 98:411–454, 1992.

[31] L.L. Thompson and P.M. Pinsky. A Galerkin least squares finite element method for the two-dimensional Helmholtz equation. *Int. J. Numer. Methods Engng.*, 38:371–397, 1995.

[32] D. Givoli. Non-reflecting boundary conditions: A review. *J. Comput. Phys.*, 94:1–29, 1991.

[33] N.N. Abboud. *A mixed finite element formulation for the transient and harmonic exterior fluid-structure interaction problem*. PhD thesis, Stanford University, August 1990.

[34] J.B. Keller and D. Givoli. Exact non-reflecting boundary conditions. *J. Comput. Phys.*, 82(1):172–192, 1989.

[35] M. Grote and J.B. Keller. Exact non-reflecting boundary conditions for the time-dependent wave equation. *SIAM Appl. Math.*, 55(2):280–297, April 1995.

[36] M.C. Junger and D. Feit. *Sound, Structures and their Interaction*. M.I.T. Press, Cambridge, MA, 1986.

[37] D. Givoli and J.B. Keller. Non-reflecting boundary conditions for elastic waves. *Wave Motion*, 12:261–279, 1990.

[38] I. Harari. *Computational Methods for Problems of Acoustics with Particular Reference to Exterior Domains*. PhD thesis, Stanford University, 1991.

[39] B. Engquist and A. Majda. Absorbing boundary conditions for the numerical simulation of waves. *Math. Comput.*, 31:629–652, 1977.

[40] B. Engquist and A. Majda. Radiation boundary conditions for acoustic and elastic calculations. *Commun. Pure Appl. Math.*, 32:313–357, 1979.

[41] D. Givoli and J.B. Keller. Special finite elements for use with high-order boundary conditions. *Comp. Methods in Applied Mech. Engng.*, 119:199–213, 1994.

[42] L.F. Kallivokas, J. Bielak, and R.C. MacCamy. Symmetric local absorbing boundaries in time and space. *ASCE J. Eng. Mech.*, 117(9):2027–2048, 1991.

[43] A. Bayliss, M. Gunzburger, and E. Turkel. Boundary conditions for the numerical solution of elliptic equations in exterior regions. *SIAM J. of Applied Math.*, 42(2):430–451, 1982.

[44] L.L. Thompson. A multi-field space-time finite element method for structural acoustics. In *Proc. of the 1995 Design Engineering Technical Conferences, Acoustics, Vibrations, and Rotating Machines*, volume 3. ASME 15th Biennial Conference on Mechanical Vibration and Noise, Sept. 17-21, 1995, Boston, Mass., 1995.